

# Multipole Semantic Attention: A Fast Approximation of Softmax Attention for Pretraining

Rupert Mitchell<sup>1</sup> Kristian Kersting<sup>1 2 3 4</sup>

## Abstract

Pretraining transformers on long sequences—entire code repositories, collections of related documents—is bottlenecked by quadratic attention costs. We present Multipole Semantic Attention (MuSe), which accelerates 64k-context pretraining by 36% while matching baseline loss, requiring no architectural changes. MuSe clusters queries and keys separately in representation space. This yields query-specific summaries that substantially outperform spatial blocking at matched sparsity, while also enabling drop-in compatibility with existing pretrained models—we validate on Llama 3.1-8B and 3.2-1B without retraining. We pretrain language models up to 1B parameters at 64k context on code and scientific documents, confirming that MuSe preserves quality and long-context utilization during training.

## 1. Introduction

The quadratic computational complexity of softmax attention remains the primary bottleneck limiting context length in transformers. While this  $\mathcal{O}(N^2D)$  scaling enables the rich token interactions that underpin transformer capabilities, it renders long-context pretraining prohibitively expensive. Modern pretraining increasingly benefits from extended context—whether processing entire code repositories or collections of related scientific papers—yet computational constraints force most models to train on artificially truncated sequences. Modern transformers partially mitigate these issues through the use of flash attention (Dao et al., 2022), which reduces memory complexity to linear but retains quadratic computational complexity. Hybrid

architectures using sliding window attention for local interactions must still interleave quadratic-complexity global attention layers to maintain full-context understanding. Efficient approximations to global attention, which maintain training quality at these scales, become essential for practical long-context pretraining.

In this context, we present Multipole Semantic Attention (MuSe), combining semantic clustering with ideas from computational physics to approximate softmax attention. We demonstrate that (1) the approximation matches or exceeds baseline training quality, (2) throughput improvements of 36% are achievable with current hardware at context lengths of 64k, and (3) the method integrates into existing training pipelines without architectural changes. More specifically, MuSe introduces three key elements: First, we cluster queries and keys separately in their learned representation spaces, enabling a two-stage mechanism where coarse query clusters attend to fine key clusters, then fine queries refine through cluster summaries. Second, we augment centroid-based (monopole) approximations with retrieval of the most relevant clusters for exact attention. Third, query centroids provide exponential tilts that center the approximation around each query cluster’s region of attention, enabling drop-in compatibility with existing pretrained models without retraining.

This distinction between the key and query latent spaces, whereby we cluster keys and queries independently, is motivated as follows. Firstly, softmax attention is invariant under translation of the keys (as this change is absorbed by the normalizing constant), but not of the queries. More importantly, the queries live in the dual vector space to the keys, that is, softmax attention is further invariant to an arbitrary change of basis of the keys, so long as the queries are transformed inversely. The consequence of this is that, unless one has some way to choose a preferred basis, it is unclear what it would mean to say that some particular key and query occupied the same point in latent space.

We validate MuSe empirically through microbenchmarks and end-to-end pretraining at scale. On isolated attention layers, we achieve 2 $\times$  speedup compared to CUDNN Flash Attention at 64k context with approximation errors below 1%. We pretrain 1B parameter models on 64k context using

<sup>1</sup>Department of Computer Science, TU Darmstadt, Darmstadt, Germany <sup>2</sup>Hessian Center for AI (hessian.AI), Darmstadt, Germany <sup>3</sup>German Research Center for Artificial Intelligence (DFKI), Darmstadt, Germany <sup>4</sup>Center for Cognitive Science, TU Darmstadt, Darmstadt, Germany. Correspondence to: Rupert Mitchell <mail@rupertmitchell.com (institutional: rupert.mitchell@tu-darmstadt.de)>.

both code repositories and scientific documents, demonstrating 36% wall-clock speedup while matching baseline quality. We further validate that the method generalizes to existing pretrained models (Llama 3.1-8B and 3.2-1B) and confirm that our models utilize the full 64k context during training.

To summarize, this paper makes the following contributions:

- A bidirectional semantic clustering approach that partitions queries and keys *separately* in their native representation space, enabling a hierarchical two-stage attention mechanism: coarse query clusters first attend to all fine key clusters to produce query-dependent summaries, then fine queries refine these summaries using their residual components
- A retrieval-augmented approximation that selects the most relevant key-value clusters for exact attention, with causal accumulation of summaries across spatial blocks
- Empirical validation at 1B parameter scale on code and scientific documents with 64k context, achieving 36% wallclock speedup while maintaining training quality

## 2. Related Work

We organize existing efficient attention methods into two broad categories: those which restrict attention to subsets of tokens exactly, and those which approximate attention globally. We fall into the latter category, and together with Hooper et al. (2025a) are the only works using semantic clustering therein.

**Restricted Attention** Reformers (Kitaev et al., 2020) bucket queries and keys according to random directions and restrict attention to within buckets. Routing Transformers (Roy et al., 2021) learn a k-means clustering during training and similarly restrict attention to within buckets. Since late 2024 there has been significant work on K-means clustering in key-space for inference acceleration: Hooper et al. (2025b) use context-specific clustering to perform exact attention on the most relevant keys, while Tactic (Zhu et al., 2025) adapts the number of retrieved tokens to attention temperature.

**Approximate Attention** Wang et al. (2020) use random projections to approximate the attention matrix, exploiting its low rank structure. Nyströmformer (Xiong et al., 2021) constructs a low rank representation using segment-wise means as landmarks. Fast Multipole Attention (Kang et al., 2023) and H-Transformer (Zhu & Soricut, 2021) use recursive spatial decomposition inspired by Barnes-Hut simulation (Barnes, 1986). Performer (Choromanski et al., 2021)

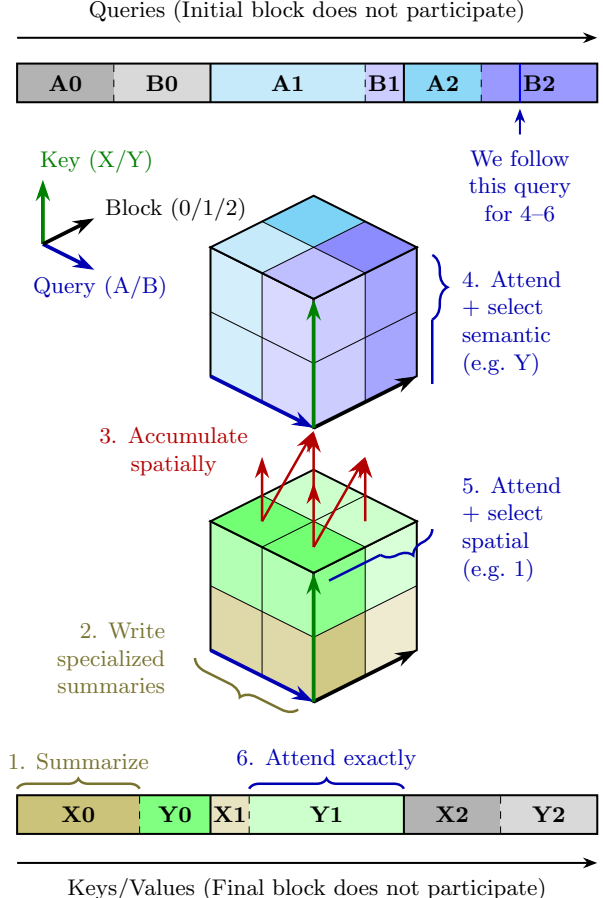


Figure 1. MuSe method overview, depicting the far-field approximation. **Bars:** Queries (top) and keys/values (bottom) are partitioned by semantic cluster (A/B for queries, X/Y for keys) within each spatial block (0, 1, 2); segments vary in size because cluster membership is data-dependent. **Lower cube:** Per-block summaries indexed by (query cluster, key cluster, spatial block), constructed in Steps 1–2. **Upper cube:** Causally accumulated summaries (Step 3), accumulated along the spatial axis. **Steps 4–6:** A query in segment B2 (blue line) attends to the upper cube to select key cluster Y (Step 4, semantic selection), then to the lower cube to select spatial block 1 (Step 5, spatial selection), and finally attends exactly to keys in (Y, 1) (Step 6). Greyed-out segments do not participate: the first query block has no prior context, and the final key/value block is only accessed via local attention (computed separately). See Algorithm 1 for pseudocode.

uses random features to approximate the exponential kernel. Mixture of Blocks Attention (MoBA; Lu et al., 2025) uses fixed spatial blocks without semantic clustering.

**Positioning of MuSe** Our work uses semantic clustering of key-query representation space. Unlike sparse training methods such as MoBA that attend to fixed spatial blocks, we compute summaries of all clusters and augment with retrieval of high-attention clusters for exact computation. Unlike Hooper et al. (2025a) who apply monopole sum-

maries at inference time with key clustering only, we target pretraining where massively parallel queries make query clustering practical: computing query-specific summaries amortizes well while substantially improving approximation quality. Crucially, MuSe requires no architectural changes: the approximation is compatible with pretrained models (validated on Llama) and MuSe-trained models switch to exact attention with minimal adaptation.

### 3. Multipole Semantic Attention (MuSe)

Softmax attention is quadratic because every query attends to every key. The core idea of MuSe is to group both queries and keys by “semantic” similarity—similarity in the post-position-encoding representation space seen by attention—rather than solely by sequence position (key clusters depicted as green circles in Figure 2). Clustering queries separately from keys enables query-specific summaries that tightly approximate attention while remaining interchangeable with exact attention at test time. We combine this with spatial blocking for causality and selective retrieval of important (cluster, block) pairs for exact attention.

The core data structure is a summaries tensor of shape  $C_q \times C_k \times (N/B)$ , where  $C_q$  and  $C_k$  are the number of query and key clusters (typically  $C_q = C_k = C$ ), and  $N/B$  is the number of spatial blocks. Each entry summarizes the keys and values in a specific (query cluster, key cluster, spatial block) triple, enabling efficient approximate attention with selective exact retrieval.

**Spatial blocks** The context of length  $N$  is divided into  $N/B$  spatial blocks of size  $B$  (e.g., 8 blocks of 8k tokens for 64k context). This structure enables causal masking at block granularity and provides the second level of retrieval.

**Clustering** Queries and keys are clustered *globally* across the full context using a single pass of mini-batch K-means followed by a final assignment (see Appendix C), ignoring block boundaries. Each query  $q$  decomposes as  $q = \bar{q}_i + \tilde{q}$  where  $\bar{q}_i$  is the centroid of its assigned cluster  $i$  and  $\tilde{q}$  is the residual. Clustering queries separately from keys—rather than clustering only keys as in prior work—is a central contribution.

Standard softmax attention computes, for each query  $q$ :

$$Z = \sum_k \exp(q \cdot k) \quad (1)$$

$$o = Z^{-1} \sum_k \exp(q \cdot k) v_k \quad (2)$$

As we show next, MuSe approximates the majority of these exponential weights by dropping the interaction between query and key residuals. The result is accurate provided that any weights carrying large fractional error contribute negligibly to it.

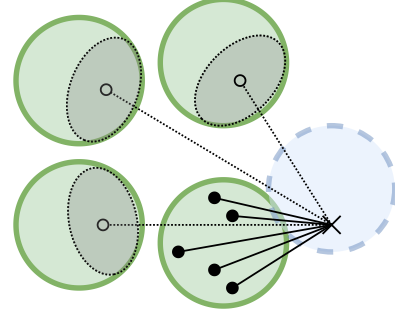


Figure 2. Geometric interpretation of MuSe. Green circles represent key/value clusters; the blue dashed circle represents a query cluster. Hollow dots mark the exponentially-tilted centroids—cluster summaries shifted toward the query cluster. Solid dots mark individual key/value pairs selected for exact retrieval. The chosen query ( $\times$ ) connects to tilted centroids via dotted lines (approximate attention) and to retrieved tokens via solid lines (exact attention).

**Why separate query clustering helps?** Consider the attention weight  $\exp(q \cdot k)$  with  $q = \bar{q} + \tilde{q}$  and  $k = \bar{k} + \tilde{k}$ . Expanding the dot product:  $\exp(q \cdot k) =$

$$\exp(\bar{q} \cdot \bar{k} + \bar{q} \cdot \tilde{k} + \tilde{q} \cdot \bar{k} + \tilde{q} \cdot \tilde{k}) \approx \exp(\bar{q} \cdot \bar{k} + \bar{q} \cdot \tilde{k} + \tilde{q} \cdot \bar{k}) \quad (3)$$

If we cluster only keys (approximating  $k \approx \bar{k}$ ), we lose the two terms involving  $\tilde{k}$ . With both query and key clustering, our two-stage mechanism retains three of four terms, dropping only  $\tilde{q} \cdot \tilde{k}$ —the product of two residuals. On our 1B model, this tighter approximation reduces monopole error by 4–5× (Table 3). Table 2 confirms both that query clustering provides a  $\sim 9\times$  effective cluster count advantage, and that finer clustering consistently reduces error by shrinking residual magnitudes.

#### 3.1. Summary Computation and Causal Accumulation

We compress keys and values into compact cluster summaries—the monopole approximation—specialized for each query cluster via exponential tilting. These are then accumulated causally across spatial blocks.

**Per-block summaries** For each spatial block  $b$ , we compute summaries for all (query cluster  $i$ , key cluster  $j$ ) pairs by attending from the query centroid  $\bar{q}_i$  to all keys in block  $b$  that belong to cluster  $j$ . Let  $S_{ijb} = \sum_{k \in (b,j)} \exp(\bar{q}_i \cdot k)$  denote the unnormalized attention mass. The summaries are:

$$\bar{k}_{ijb} = S_{ijb}^{-1} \sum_{k \in (b,j)} \exp(\bar{q}_i \cdot k) k \quad (4)$$

$$\bar{v}_{ijb} = S_{ijb}^{-1} \sum_{k \in (b,j)} \exp(\bar{q}_i \cdot k) v \quad (5)$$

$$\bar{\mu}_{ijb} = \log S_{ijb} \quad (6)$$

These are “exponentially tilted” centroids—weighted by attention from the query centroid, not simple averages (shown

as hollow dots in Figure 2, shifted toward the query cluster). This constitutes exact attention from coarse queries to fine keys. The cost is  $\mathcal{O}(C \cdot N \cdot D)$ —linear in context length, compared to  $\mathcal{O}(N^2 D)$  for exact attention—and produces  $(N/B) \times C_q \times C_k$  summaries (Steps 1–2 in Figure 1).

**Causal accumulation** To enable causal attention, we accumulate summaries along the spatial axis so that block  $b$  has access to summaries of all preceding blocks  $0, \dots, b-1$ . The accumulation is *exclusive*—a block does not include itself:

- $\bar{\mu}$ : cumulative logsumexp
- $\bar{k}, \bar{v}$ : cumulative softmax-weighted sum (weights derived from accumulated  $\bar{\mu}$ )

After accumulation, accumulated <sub>$ijb$</sub>  summarizes all keys/values in blocks  $0 \dots b-1$  belonging to key cluster  $j$ , specialized for query cluster  $i$  via exponential tilting (Step 3 in Figure 1).

We implement this sequentially rather than with parallel scan (prefix sum), since there is already massive parallelism from  $C_q \times C_k \times \text{heads} \times \text{batch}$  independent accumulations.

### 3.2. Two-Level Retrieval

The monopole approximation (Equation 1) drops the residual cross term  $\tilde{q} \cdot \tilde{k}$ . This error is significant only when the residual query has large positive dot product with keys in a cluster. Retrieval selects exactly these clusters for exact token-level attention; for the remaining clusters, keys either carry negligible attention weight or have small residual interaction, so the monopole approximation holds. Intuitively, if the attention pattern is smooth, weighted centroids approximate it well; if it is sharp, the high-weight keys are few and retrieval captures them. This decomposition—approximating smooth interactions, computing sharp ones exactly—mirrors the Fast Multipole Method (Rokhlin, 1985), with relevance in representation space playing the role of spatial distance. This proceeds in two stages: first selecting *clusters*, then selecting *spatial blocks* within those clusters.

**Cluster selection** For each query  $q = \bar{q}_i + \tilde{q}$  in spatial block  $b$ , we compute attention scores to all  $C_k$  accumulated cluster summaries:

$$\text{score}_j = \tilde{q} \cdot \bar{k}_{ijb} + \bar{\mu}_{ijb} \quad (7)$$

This is the best available estimate of the log attention mass that query  $q$  will receive from cluster  $j$ . We select the top- $k_1$  clusters for exact retrieval (e.g.,  $k_1 = 8$  out of  $C = 128$ ), mask them out pre-softmax, and compute approximate attention over the remaining  $C - k_1$  clusters (Step 4 in Figure 1).

**Spatial block selection** For queries that selected cluster  $j$ , we now select which spatial blocks within cluster  $j$  to retrieve. This uses the *pre-accumulation* per-block summaries rather than the accumulated ones.

Queries are segmented by which cluster(s) they are retrieving. For queries in query cluster  $i$  that selected key cluster  $j$ , we attend to the  $N/B$  per-block summaries for the  $(i, j)$  pair, apply a block-index causal mask ( $b_q > b_k$ ), and select the top- $k_2$  spatial blocks (e.g.,  $k_2 = 1$  out of  $N/B = 8$ ). Selected blocks are masked out pre-softmax, and we compute approximate attention over the remaining blocks (Step 5 in Figure 1).

The output specifies  $k_1 \times k_2$  (cluster, block) pairs per query for exact retrieval (e.g.,  $8 \times 1 = 8$  pairs).

**Dipole corrections** An alternative to retrieval is to improve the monopole (centroid) approximation with higher-order terms. By expanding attention as a polynomial in  $\tilde{q}$ , one obtains a dipole correction involving the covariance  $\text{Cov}(v, k)$  within each cluster, reducing approximation error from  $\mathcal{O}(\tilde{q} \cdot \tilde{k})$  to  $\mathcal{O}(\tilde{q}^2 \cdot \tilde{k}^2)$ . We derive this in Appendix B. In practice, retrieval provides larger accuracy gains at acceptable computational cost (see Appendix B for an empirical comparison), so we use retrieval in our main experiments.

### 3.3. Exact Retrieval and Local Attention

The retrieved (cluster, block) pairs and the local block diagonal are computed with exact flash attention, recovering token-level detail that the monopole summaries cannot capture.

**Exact retrieval** We perform exact flash attention from each query to its selected (cluster, block) pairs, using the *full query* (not the residual) (Step 6 in Figure 1). Keys and values are bucketed by (cluster, block). We build an inverse index mapping each (cluster, block) to the queries that retrieve it, then perform segmented flash attention.

To avoid  $k_1 \times k_2$  memory blowup, we use index arrays into the original queries, keys, and values rather than materializing expanded arrays, similar to the segmentation approach in FlashMoBA (Xiao et al., 2025).

**Local attention** For within-block attention (the “diagonal”), we use exact flash attention with standard causal masking. This handles local interactions where attention is typically strongest. (Figure 1 depicts only the far-field approximation; local attention is computed separately.)

**Output merging** The final output merges four components via logsumexp weighting:

1. Approximate attention from non-retrieved clusters

(from cluster selection)

2. Approximate attention from non-retrieved blocks within retrieved clusters (from block selection)
3. Exact attention from retrieved (cluster, block) pairs
4. Exact local attention within the current block

**Complexity** At our operating point (64k context, 8k block diagonal), the block diagonal contributes 1/8 of full quadratic cost, with the far-field approximated at  $64 \times$  sparsity. Maintaining these ratios as context scales, we find approximation error decreases substantially (Appendix F.5); quantifying the resulting speedups at longer contexts is future work. With typical parameters ( $N = 2^{16}$ ,  $C = 128$ ,  $B = 8192$ ,  $k_1 = 8$ ,  $k_2 = 1$ ), we achieve significant speedups both in theoretical FLOPs and in wall-clock time (Section 4). We implement MuSe in JAX with custom Pallas kernels for summary computation and segmented retrieval, and CUDA kernels for K-means clustering (Appendix C). The approximation is compatible with standard distributed training strategies (Appendix G.4).

## 4. Experiments

### 4.1. Setup and Microbenchmarks

**Runtime Comparison** Table 1 compares attention runtime across methods on the 1B model (64 heads, 2 sequences of 64k context each). MuSe achieves  $2 \times$  speedup over CUDNN Flash Attention while maintaining high approximation quality. We also compare against MoBA at matched far-field sparsity: both methods use an 8k block diagonal, and MoBA retrieves one 512-token block per query to match MuSe’s retrieval of 8 clusters  $\times$  1 spatial block ( $\sim 512$  tokens). MoBA is slightly faster than MuSe (no summarization overhead), but MuSe achieves  $40 \times$  lower approximation error (0.006 vs 0.248 relative squared error).

**Table 1. MuSe achieves  $2 \times$  speedup with  $40 \times$  lower error than MoBA at matched sparsity.** Attention runtime comparison (1B model, 64 heads,  $2 \times 64k$  context).  $^\dagger$ Matched sparsity: 8k block diagonal,  $64 \times$  far-field.

Method	Time (ms)	Speedup	RSE
CUDNN Flash	225.6	1.00 $\times$	0 (exact)
Pallas Flash	265.6	0.85 $\times$	0 (exact)
MuSe (Ours) $^\dagger$	114.1	1.98 $\times$	<b>0.006</b>
MoBA $^\dagger$	109.0	2.07 $\times$	0.248
Block diag. only	35.0	6.45 $\times$	0.481

**1B Model Validation** Table 2 validates the query clustering benefit on our headline 1B parameter model (320 heads, head dimension 64). We vary cluster count jointly ( $Q=K$ ) with retrieval fraction fixed at  $R/QK = 1/16$ . For each

configuration, we compute the effective no-query-clustering cluster count—the cluster count the ablated method would require to achieve the same error, interpolated via power-law fit. MuSe exhibits a steeper power-law slope ( $d \approx -0.89$ ) than the no-query-clustering ablation ( $d \approx -0.59$ ), so the effective cluster multiplier grows with cluster count: from 5.1 $\times$  at QK16 to 10.7 $\times$  at QK512. At our operating point of QK128R8, MuSe achieves error that would require  $\sim 1200$  clusters without query clustering—a 9.2 $\times$  effective cluster count advantage.

**Table 2. Query clustering provides a  $\sim 9 \times$  effective cluster count advantage.** MuSe approximation quality on 1B model (320 heads, 2 sequences, 64k context).  $R = QK/16$  throughout. Timing measured on 40 heads due to memory constraints. Effective No-Q cluster count computed via power-law interpolation; values marked with  $\dagger$  are extrapolated beyond measured No-Q data (QK512).

QK	RSE	Corr	Eff. No-Q	Mult.	Time (ms)
16	0.03797	0.9775	82	5.1 $\times$	—
32	0.02100	0.9878	191	6.0 $\times$	130.0
64	0.01139	0.9935	568 $\dagger$	8.9 $\times$	88.5
<b>128</b>	<b>0.00622</b>	<b>0.9965</b>	<b>1179<math>\dagger</math></b>	<b>9.2<math>\times</math></b>	<b>80.5</b>
256	0.00330	0.9980	2518 $\dagger$	9.8 $\times$	106.8
512	0.00173	0.9990	5481 $\dagger$	10.7 $\times$	219.8

**Monopole vs Retrieval Decomposition** To understand where query clustering helps, we measure approximation quality for monopole-only (no retrieval) and retrieval-only (no monopole) variants on the 1B model. Table 3 shows that query clustering dramatically improves monopole quality (3.7–5.6 $\times$  error reduction) but barely affects retrieval selection (1.02 $\times$ ). This confirms that query clustering improves the *quality* of cluster summaries; retrieval selection works well either way because it only needs to identify high-attention clusters, not compute precise values.

**Table 3. Query clustering acts through improved cluster summaries, not retrieval selection.** Monopole vs retrieval decomposition on 1B model. “With Q” uses query clustering; “No Q” uses zeroed query centroids. Query clustering provides 4.5 $\times$  benefit for monopole but only 1.02 $\times$  for retrieval.

Component	Setting	RSE	Corr	Q benefit
Monopole (K64)	With Q	0.0342	0.9795	3.7 $\times$
	No Q	0.1278	0.9282	
Monopole (K128)	With Q	0.0227	0.9866	4.5 $\times$
	No Q	0.1016	0.9426	
Monopole (K256)	With Q	0.0148	0.9913	5.6 $\times$
	No Q	0.0824	0.9534	
Retrieval (K128R8)	With Q	0.2429	0.9407	1.02 $\times$
	No Q	0.2475	0.9367	

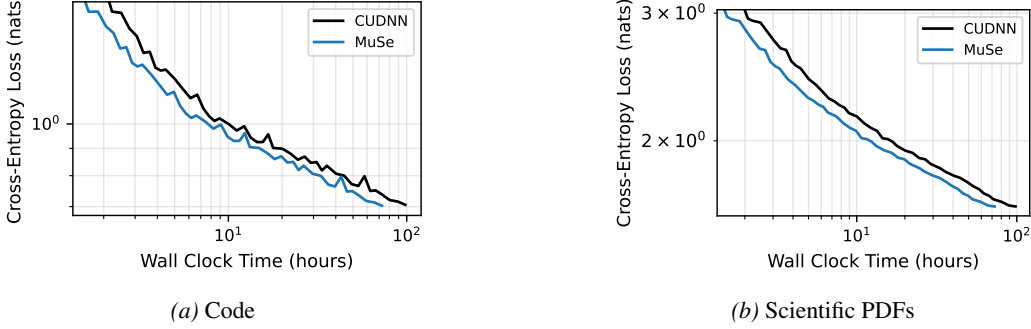


Figure 3. Training loss versus wall-clock time for 1B models on code (left) and scientific PDF (right) domains. MuSe (blue) and CUDNN (black) follow the same loss trajectory, shifted horizontally—the gap is the 36% throughput advantage. Plots start after warmup (4000 steps). Trained on a single node of 8 NVIDIA A100 GPUs.

Table 4. MuSe matches or beats the CUDNN baseline on both domains. Headline 1B results on code (24B tokens) and scientific PDFs (24B tokens). Cross-entropy loss, lower is better.  $^\dagger$ Fine-tuned with CUDNN attention for 0.1% of pretraining tokens.

Domain	Train	Test Attention	
		CUDNN	MuSe
Code	CUDNN	0.7026	—
Code	MuSe	0.7108	0.7001
Code	MuSe $^\dagger$	<b>0.6994</b>	0.7020
PDF	CUDNN	1.6201	—
PDF	MuSe	<b>1.6166</b>	1.6188

## 4.2. Pretraining Results

**Headline Results** Table 4 summarizes our main 1B parameter results on both code and scientific PDF domains. On code, MuSe achieves a train-MuSe/test-MuSe loss of 0.7001 compared to the CUDNN baseline of 0.7026 (0.4% improvement). When tested with CUDNN attention, there is a small adaptation gap (0.7108, 1.2% degradation); however, this gap closes rapidly with brief CUDNN fine-tuning: after just 26M tokens ( $\sim 0.1\%$  of pretraining), the fine-tuned model achieves 0.6994, *beating* the baseline (see Appendix G.3 for details). On scientific PDFs, MuSe outperforms the baseline: 1.6166 vs 1.6201 (0.2% improvement), with minimal interchangeability gap (1.6188 when tested with MuSe attention). We hypothesize two competing effects: the approximation acts as implicit regularization (improving generalization), while extended training allows minor adaptation to the approximation’s specific behavior. The regularization effect dominates early and at smaller scales, explaining why MuSe beats the baseline; adaptation emerges with extended training but is easily removed via fine-tuning.

**Speedup Analysis** At 1B scale on a single node of 8 A100 GPUs with 64k context, MuSe achieves 88.9 KTok/s compared to 65.3 KTok/s for CUDNN Flash Attention—a **36% throughput improvement**. Our Pallas kernels are

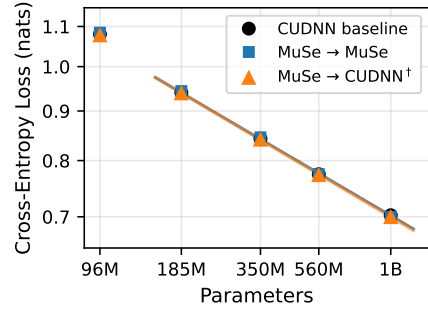


Figure 4. Scaling behavior from 96M to 1B parameters. Power law fits (lines) span 185M–1B, where scaling is cleanest; the 96M point falls slightly above the fit. MuSe-trained models evaluated with CUDNN attention (orange triangles,  $^\dagger$ ) track the exact attention baseline, confirming that the approximation preserves scaling properties.  $^\dagger$ The 1B point uses the fine-tuned value after 0.1% additional CUDNN training.

not highly optimized relative to production-quality CUDA; substantially larger speedups are achievable given the  $64\times$  far-field sparsity. Combined with the minimal quality degradation shown above, this demonstrates that MuSe provides substantial practical speedups for long-context pretraining.

Figure 3 shows training loss versus wall-clock time on both code and scientific PDF domains. At any given loss level, MuSe reaches that point faster than CUDNN, with the horizontal gap representing the throughput advantage. The curves are nearly identical when plotted against tokens (see Appendix), confirming that MuSe achieves equivalent sample efficiency—the speedup comes purely from faster iteration, not from any change in learning dynamics.

**Scaling Analysis** Table 5 and Figure 4 present scaling results on the code domain from 96M to 1B parameters. We train each model for approximately 20 tokens per parameter, following compute-optimal scaling (Hoffmann et al., 2022). We report cross-entropy loss for models trained with either CUDNN Flash Attention or MuSe, evaluated with both at-

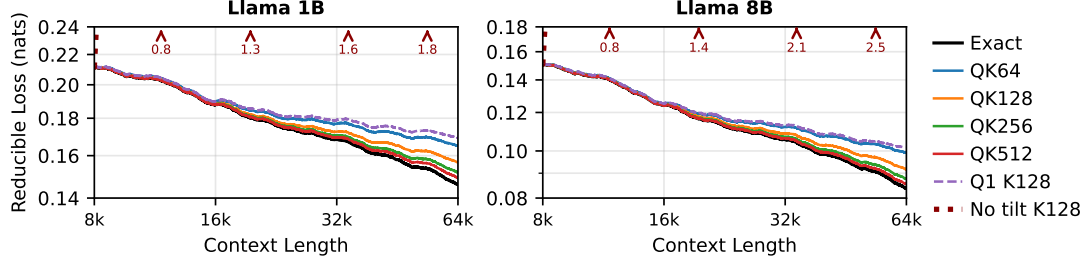


Figure 5. Cumulative mean loss versus context length on Project Gutenberg text for Llama 3.2-1B (left) and Llama 3.1-8B (right). MuSe with various cluster counts (QK64–QK512) tracks exact attention closely, with the gap reducing by  $\sim 1.8\times$  per doubling for 1B and  $\sim 2\times$  for 8B. Without exponential tilting (“No tilt K128”, dotted), loss explodes immediately. Query clustering provides additional benefit: QK64 outperforms Q1 K128 despite using half the key clusters, demonstrating that clustering queries more than doubles practical quality. Y-axes show reducible loss (cumulative mean minus fitted irreducible loss: 2.30 nats for 1B, 1.96 nats for 8B).

Table 5. MuSe matches baseline scaling laws across five model sizes. Scaling results on code domain (cross-entropy loss). Lower is better.  $^\dagger$ Fine-tuned with CUDNN attention for 0.1% of pretraining tokens.

Params	Train	Test Attention	
		CUDNN	MuSe
1B	CUDNN	0.7026	—
1B	MuSe	0.7108	0.7001
1B	MuSe $^\dagger$	<b>0.6994</b>	0.7020
560M	CUDNN	0.7745	—
560M	MuSe	<b>0.7728</b>	0.7746
350M	CUDNN	0.8427	—
350M	MuSe	<b>0.8407</b>	0.8453
185M	CUDNN	0.9400	—
185M	MuSe	<b>0.9384</b>	0.9435
96M	CUDNN	1.080	—
96M	MuSe	<b>1.077</b>	1.084

tention methods to assess interchangeability. At scales up to 560M, MuSe-trained models match or exceed the CUDNN baseline when evaluated with CUDNN attention. At 1B scale, MuSe-trained models tested with MuSe attention beat the baseline (0.7001 vs 0.7026), though there is minor adaptation when tested with CUDNN attention (0.7108); this adaptation is removed with brief CUDNN fine-tuning (0.1% of pretraining tokens), after which the model beats the baseline even when tested with CUDNN attention (0.6994 vs 0.7026). Power law fits to the 185M–1B data (excluding the undertrained 96M point) show that MuSe follows the same scaling law as exact attention (loss  $\propto$  params $^{-0.17}$ ,  $R^2 > 0.999$ ).

**Method Comparison** Table 6 compares MuSe against MoBA at 185M and 560M scale with matched sparsity (8k block diagonal, 64 $\times$  far-field sparsity). MoBA uses spatial block structure without semantic clustering, retrieving one 512-token block in the far field per query to achieve the

Table 6. MuSe beats the exact baseline; MoBA does not. Method comparison at 185M and 560M scale (cross-entropy loss). All methods use matched sparsity (8k block diagonal, 64 $\times$  far-field sparsity). Lower is better.

Method	Test Attention	
	CUDNN	Method
185M: CUDNN (baseline)	0.9400	—
MuSe	<b>0.9384</b>	0.9435
MoBA	0.9714	1.0027
560M: CUDNN (baseline)	0.7745	—
MuSe	<b>0.7728</b>	0.7746
MoBA	0.7958	0.8209

matched sparsity.

MuSe is the only method that *beats* the exact CUDNN baseline at both scales (0.9384 vs 0.9400 at 185M; 0.7728 vs 0.7745 at 560M), demonstrating that our approximation can act as a beneficial regularizer. MoBA performs significantly worse at both scales (0.9714 at 185M, 0.7958 at 560M), showing that semantic clustering—not just sparsity—is critical for approximation quality. Even if MoBA reallocates compute from the block diagonal to reduce far-field sparsity to 8 $\times$ , MuSe maintains an advantage (Appendix F.4). The importance of query clustering is discussed further in Section 4.3.

**Head Dimension** Following recent open-weight releases from major labs (OpenAI, 2025), our main experiments use head dimension 64. Table 7 validates that MuSe also works well with head dimension 128, as used by Llama models. At 185M scale, MuSe with head dimension 128 slightly outperforms the CUDNN baseline (0.9113 vs 0.9121) and shows strong interchangeability. Microbenchmarks confirm similar approximation quality: at our operating point (QK128R8), head dimension 128 achieves 0.0100 relative squared error

and 0.994 correlation, compared to 0.0094 and 0.995 for head dimension 64.

**Table 7. MuSe generalizes to head dimension 128.** Head dimension 128 comparison at 185M/4B scale (cross-entropy loss).

Train	Test Attention	
	CUDNN	MuSe
CUDNN	0.9121	0.9267
MuSe	<b>0.9113</b>	0.9159

**Downstream Evaluation** As a sanity check, we evaluate 1B models on ARC-Easy and SciQ using the lm-eval harness. MuSe-trained and CUDNN-trained models perform comparably (e.g., 48.7% vs 47.9% on ARC-Easy), with all differences within one standard error, confirming that the approximation does not impair downstream task performance (full results in Appendix G.2).

### 4.3. Generalization and Long-Context Validation

To validate that MuSe generalizes beyond models trained with it, we evaluate on pretrained Llama 3.2-1B (head dimension 64) and Llama 3.1-8B (head dimension 128) using 64k-token passages from Project Gutenberg.

**Evaluation on Existing Models** Figure 5 shows cumulative mean loss as a function of context length. With tilting enabled, all MuSe configurations track exact attention with modest gaps that decrease with cluster count. The gap approximately halves with each doubling of QK clusters, and QK512 nearly matches exact attention for both models.

Critically, without exponential tilting by query centroids (“No tilt K128”), loss explodes immediately—the approximation fails catastrophically on pretrained models. This demonstrates that tilting is essential for drop-in compatibility: attention heads with non-trivial mean query values cannot be approximated without accounting for this bias.

Query clustering provides substantial additional benefit beyond tilting alone. Comparing Q1 K128 (single query cluster with tilting) to QK64 (64 query and key clusters), QK64 achieves lower error despite using half as many key clusters. This shows that clustering queries more than doubles the effective quality of the approximation. This benefit comes at negligible cost: attention with few queries is memory-bound, with operational intensity approximately proportional to the query count (Ye et al., 2025), so tilting by moderate numbers of centroids (32–64) is essentially free on current hardware.

**Context Utilization During Training** Figure 6 demonstrates that models trained with MuSe learn to utilize the full 64k context throughout training. Loss continues to decrease with position even beyond the approximation threshold at

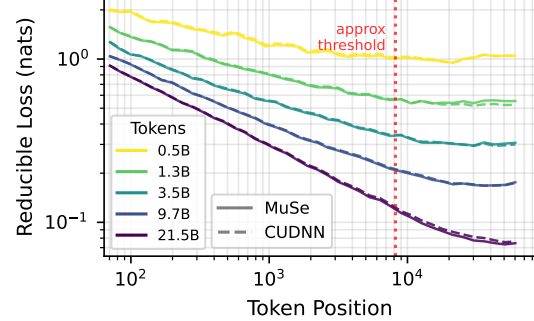


**Figure 6.** Loss versus position during 1B model training on code data. Curves show progression from early training (light) to late training (dark) at 5 checkpoints spanning 0.5B to 21.5B tokens. MuSe (solid) closely tracks cuDNN attention (dashed) throughout training. The vertical line marks  $2^{13} = 8192$  tokens, beyond which MuSe uses far-field approximation. Both methods learn to utilize the full 64k context, with loss continuing to decrease even in the approximated region.

$2^{13}$  tokens, where MuSe transitions from exact to far-field computation. The close correspondence between MuSe and exact attention at all training stages confirms that the approximation does not impair the model’s ability to learn long-range dependencies.

## 5. Conclusion

We have presented Multipole Semantic Attention (MuSe), an efficient approximation to softmax attention that clusters queries and keys separately in their learned representation spaces. By computing query-specific cluster summaries and augmenting with retrieval of high-attention clusters, MuSe achieves  $64 \times$  far-field sparsity with under 1% relative squared error.

Our experiments demonstrate practical benefits at scale:  $2 \times$  speedup over CUDNN Flash Attention on isolated attention layers, and 36% wallclock throughput improvement when pretraining 1B parameter models at 64k context. Models trained with MuSe achieve comparable loss to exact attention baselines and remain interchangeable at test time. Exponential tilting by query centroids is essential for compatibility with pretrained models, and query clustering provides substantial additional quality at negligible cost.

Limitations include the focus on head dimension 64 in most experiments, though preliminary results at dimension 128 are promising. Future work includes scaling to larger models, kernel optimization, and investigating whether query-dependent tilting benefits other approximate attention mechanisms. We currently compute summaries independently per head; for grouped-query attention (GQA), reusing key/value summaries across query heads within a group is a natural further optimization.

## Acknowledgements

This work was supported by the Hessian research priority programme LOEWE within the project “WhiteBox”, and the Aleph Alpha Collaboration Lab 1141. It benefited from the Federal Ministry for Research, Technology and Space (BMFTR) project “XEI: Extremely Efficient Inference for Large Context Length” (XEI), project identification number 01IS24079B, and from funding by the Deutsche Forschungsgemeinschaft (DFG, German Research Foundation) under Germany’s Excellence Strategy – EXC-3057. We thank Manuel Brack, Moritz Willig, Felix Friedrich, Felix Divo, Florian Busch, and Rubin Härtle for helpful discussions and feedback on the manuscript.

## References

Barnes, H. A hierarchical  $O(n \log n)$  force-calculation algorithm. *Nature*, 1986.

Choromanski, K. M., Likhoshesterov, V., Dohan, D., Song, X., Gane, A., Sarlós, T., Hawkins, P., Davis, J. Q., Mo-hiuddin, A., Kaiser, L., Belanger, D. B., Colwell, L. J., and Weller, A. Rethinking attention with performers. In *ICLR*. OpenReview.net, 2021.

Dao, T., Fu, D. Y., Ermon, S., Rudra, A., and Ré, C. Flashattention: Fast and memory-efficient exact attention with io-awareness. In *NeurIPS*, 2022.

Hoffmann, J., Borgeaud, S., Mensch, A., Buchatskaya, E., Cai, T., Rutherford, E., de Las Casas, D., Hendricks, L. A., Welbl, J., Clark, A., Hennigan, T., Noland, E., Millican, K., van den Driessche, G., Damoc, B., Guy, A., Osindero, S., Simonyan, K., Elsen, E., Rae, J. W., Vinyals, O., and Sifre, L. Training compute-optimal large language models. In *NeurIPS*, 2022.

Hooper, C., Zhao, S., Manolache, L., Kim, S., Mahoney, M. W., Shao, Y. S., Keutzer, K., and Gholami, A. Multipole attention for efficient long context reasoning. *CoRR*, abs/2506.13059, 2025a.

Hooper, C. R. C., Kim, S., Mohammadzadeh, H., Maheswaran, M., Zhao, S., Paik, J., Mahoney, M. W., Keutzer, K., and Gholami, A. Squeezed attention: Accelerating long context length LLM inference. In *ACL (1)*, pp. 32631–32652. Association for Computational Linguistics, 2025b.

Kang, Y., Tran, G., and De Sterck, H. Fast multipole attention: A divide-and-conquer attention mechanism for long sequences. *arXiv preprint arXiv:2310.11960*, 2023.

Kitaev, N., Kaiser, L., and Levskaya, A. Reformer: The efficient transformer. In *ICLR*. OpenReview.net, 2020.

Lozhkov, A., Li, R., Allal, L. B., Cassano, F., Lamy-Poirier, J., Tazi, N., Tang, A., Pykhtar, D., Liu, J., Wei, Y., Liu, T., Tian, M., Kocetkov, D., Zucker, A., Belkada, Y., Wang, Z., Liu, Q., Abulkhanov, D., Paul, I., Li, Z., Li, W.-D., Risdal, M., Li, J., Zhu, J., Zhuo, T. Y., Zheltonozhskii, E., Dade, N. O. O., Yu, W., Krauß, L., Jain, N., Su, Y., He, X., Dey, M., Abati, E., Chai, Y., Muennighoff, N., Tang, X., Oblokulov, M., Akiki, C., Marone, M., Mou, C., Mishra, M., Gu, A., Hui, B., Dao, T., Zebaze, A., Dehaene, O., Patry, N., Xu, C., McAuley, J., Hu, H., Scholak, T., Paquet, S., Robinson, J., Anderson, C. J., Chapados, N., Patwary, M., Varshney, N., Yadav, P., Salakhutdinov, R., von Werra, L., and de Vries, H. Starcoder 2 and the stack v2: The next generation. *arXiv preprint arXiv:2402.19173*, 2024.

Lu, E., Jiang, Z., Liu, J., Du, Y., Jiang, T., Hong, C., Liu, S., He, W., Yuan, E., Wang, Y., Huang, Z., Yuan, H., Xu, S., Xu, X., Lai, G., Chen, Y., Zheng, H., Yan, J., Su, J., Wu, Y., Zhang, Y., Yang, Z., Zhou, X., Zhang, M., and Qiu, J. MoBA: Mixture of block attention for long-context LLMs. In *The Thirty-ninth Annual Conference on Neural Information Processing Systems*, 2025. URL <https://openreview.net/forum?id=R1qYCpTulP>.

Olmo, T., Ettinger, A., Bertsch, A., Kuehl, B., Graham, D., Heineman, D., Groeneveld, D., Brahman, F., Timbers, F., Ivison, H., Morrison, J., Poznanski, J., Lo, K., Soldaini, L., Jordan, M., Chen, M., Noukhovitch, M., Lambert, N., Walsh, P., Dasigi, P., Berry, R., Malik, S., Shah, S., Geng, S., Arora, S., Gupta, S., Anderson, T., Xiao, T., Murray, T., Romero, T., Graf, V., Asai, A., Bhagia, A., Wettig, A., Liu, A., Rangapur, A., Anastasiades, C., Huang, C., Schwenk, D., Trivedi, H., Magnusson, I., Lochner, J., Liu, J., Miranda, L. J. V., Sap, M., Morgan, M., Schmitz, M., Guerquin, M., Wilson, M., Huff, R., Bras, R. L., Xin, R., Shao, R., Skjonsberg, S., Shen, S. Z., Li, S. S., Wilde, T., Pyatkin, V., Merrill, W., Chang, Y., Gu, Y., Zeng, Z., Sabharwal, A., Zettlemoyer, L., Koh, P. W., Farhadi, A., Smith, N. A., and Hajishirzi, H. Olmo 3, 2025. URL <https://arxiv.org/abs/2512.13961>.

OpenAI. gpt-oss-120b & gpt-oss-20b model card, 2025. URL <https://arxiv.org/abs/2508.10925>.

Rae, W., J., Potapenko, Anna, Jayakumar, M., S., Lillicrap, and P., T. Compressive transformers for long-range sequence modelling. In *ICLR*, 2020.

Rokhlin, V. Rapid solution of integral equations of classical potential theory. *Journal of Computational Physics*, 60 (2):187–207, 1985.

Roy, A., Saffar, M., Vaswani, A., and Grangier, D. Efficient content-based sparse attention with routing transformers. *Trans. Assoc. Comput. Linguistics*, 9:53–68, 2021.

Wang, S., Li, B. Z., Khabsa, M., Fang, H., and Ma, H. Linformer: Self-attention with linear complexity. *CoRR*, abs/2006.04768, 2020.

Xiao, G., Guo, J., Mazaheri, K., and Han, S. Optimizing mixture of block attention, 2025. URL <https://arxiv.org/abs/2511.11571>.

Xiong, Y., Zeng, Z., Chakraborty, R., Tan, M., Fung, G., Li, Y., and Singh, V. Nyströmformer: A nyström-based algorithm for approximating self-attention. In *AAAI*, pp. 14138–14148. AAAI Press, 2021.

Ye, Z., Chen, L., Lai, R., Lin, W., Zhang, Y., Wang, S., Chen, T., Kasikci, B., Grover, V., Krishnamurthy, A., and Ceze, L. Flashinfer: Efficient and customizable attention engine for LLM inference serving. In *Eighth Conference on Machine Learning and Systems*, 2025. URL <https://openreview.net/forum?id=RXPofAsL8F>.

Zhu, K., Tang, T., Xu, Q., Gu, Y., Zeng, Z., Kadekodi, R., Zhao, L., Li, A., Krishnamurthy, A., and Kasikci, B. Tac-tic: Adaptive sparse attention with clustering and distribution fitting for long-context llms. *CoRR*, abs/2502.12216, 2025.

Zhu, Z. and Soricut, R. H-transformer-1d: Fast one-dimensional hierarchical attention for sequences. In *ACL/IJCNLP (1)*, pp. 3801–3815. Association for Computational Linguistics, 2021.

## A. Algorithm Pseudocode

### Algorithm 1 MuSe Causal Attention

**Require:** Queries  $Q$ , Keys  $K$ , Values  $V$  of length  $N$ ; block size  $B$ ; cluster count  $C$ ; retrieval counts  $k_1, k_2$

**Ensure:** Output  $O$  of length  $N$

```

1: // Clustering (global, ignores block boundaries)
2: Cluster  $Q$  into  $C$  clusters; decompose  $q = \bar{q}_i + \tilde{q}$ 
3: Cluster  $K$  into  $C$  clusters; decompose  $k = k_j + \tilde{k}$ 
4: // Per-block summaries:  $C \times C \times (N/B)$  entries
5: for each spatial block  $b$ , query cluster  $i$ , key cluster  $j$  do
6:    $\bar{\mu}_{ijb}, \bar{k}_{ijb}, \bar{v}_{ijb} \leftarrow$  attention-weighted stats of  $(K, V)$  in  $(j, b)$  from  $\bar{q}_i$ 
7: end for
8: // Causal accumulation along spatial axis
9: for each block  $b = 1, \dots, N/B - 1$  do
10:  accumij,b  $\leftarrow$  accumij,b-1  $\oplus$  summaryij,b-1 {logsumexp merge}
11: end for
12: // Two-level retrieval + attention (per query)
13: for each query  $q$  in cluster  $i$ , block  $b$  do
14:   Select top- $k_1$  key clusters from accumi,;,b {Cluster selection}
15:   Select top- $k_2$  blocks per cluster from summaryi,j,: {Spatial selection}
16:    $O_{\text{retrieved}} \leftarrow$  exact attention on  $k_1 \times k_2$  (cluster, block) pairs
17:    $O_{\text{approx}} \leftarrow$  approximate attention on remaining clusters/blocks
18:    $O_{\text{local}} \leftarrow$  exact causal attention within block  $b$ 
19: end for
20: return logsumexp-weighted merge of  $O_{\text{retrieved}}, O_{\text{approx}}, O_{\text{local}}$ 

```

## B. Dipole Derivation

Here we present an alternative to retrieval based on polynomial expansion of the attention function, which we call the dipole correction. While retrieval performs better empirically, this derivation provides theoretical insight into the approximation.

**Polynomial Expansion via Cumulant Generating Functions** The keys  $k$  of some cluster  $j$  can be considered as a probability distribution of equally weighted point masses. They have moment generating function  $\mathcal{M}_j(q) := \mathbb{E}_{k \in C_j} \exp(q \cdot k)$  and cumulant generating function (CGF)  $\mathcal{K}_j(q) := \ln \mathcal{M}_j(q)$ , whose derivatives give the cumulants (mean, variance, skewness, etc.).

Attending to keys with query centroid  $\bar{q}_i$  corresponds to an exponential tilt of this distribution. Define the CGF of the joint key-value distribution:  $\mathcal{K}_j(q, t) := \ln \mathbb{E}_{k, v \in C_j} \exp(q \cdot k + t \cdot v)$ .

$k + t \cdot v$ ). The output of softmax attention on cluster  $j$  for query  $\bar{q}$  is:  $V_j(\bar{q}) = \frac{\partial \mathcal{K}_j(q, t)}{\partial t} \Big|_{q=\bar{q}, t=0}$ .

For a query  $q = \bar{q}_i + \tilde{q}$ , we can approximate  $V_j(q)$  by polynomial expansion around  $\bar{q}_i$ :

$$V_{ij}(\tilde{q}) = \bar{v}_{ij} + \text{Cov}_{ij}(v, k)\tilde{q} + \frac{1}{2}\tilde{q}^T \text{Skew}_{ij}(v, k, k)\tilde{q} + \dots \quad (8)$$

where  $\bar{v}_{ij}$ ,  $\text{Cov}_{ij}(v, k)$ , and  $\text{Skew}_{ij}(v, k, k)$  are cumulants of the exponentially-tilted distribution.

Similarly, the unnormalized attention weight expands as:

$$M_{ij}(\tilde{q}) = M_j(\bar{q}_i) \exp\left(\tilde{q} \cdot \bar{k}_{ij} + \frac{1}{2}\tilde{q}^T \text{Cov}_{ij}(k, k)\tilde{q} + \dots\right) \quad (9)$$

**Dipole Truncation** Retaining only terms linear in  $\tilde{q}$  gives the dipole approximation with error  $\mathcal{O}(\tilde{q}^2 \tilde{k}^2)$ . The covariance matrices  $\text{Cov}_{ij}(v, k)$  can be pre-merged across key clusters for each query cluster, reducing complexity from  $\mathcal{O}(NCD^2)$  to  $\mathcal{O}(ND^2)$ . The expected error is  $\mathcal{O}(\text{Tr}(\text{Cov}(\tilde{q}, \tilde{q}) \text{Cov}(\tilde{k}, \tilde{k})))$ —exactly the quantity minimized by K-means, motivating our clustering choice.

**Partially Specialized Dipoles** The above error bounds apply to fully specialized dipoles  $\text{Cov}_{ij}(v, k)$ , which require  $\mathcal{O}(QSD^2)$  compute to construct (where  $Q$  is the number of query clusters and  $S$  is the sequence length). To reduce this cost, we instead compute a single  $\text{Cov}_j(v, k)$  for each key cluster without the exponential tilt by  $\bar{q}_i$ , reducing construction cost to  $\mathcal{O}(SD^2)$ . This degrades the error bound from  $\mathcal{O}(\tilde{q}^2 \tilde{k}^2)$  to  $\mathcal{O}(\bar{q} \cdot \tilde{q} \cdot \tilde{k}^2)$ , introducing dependence on the query centroid magnitude. This degradation is substantial—roughly halving the error reduction relative to monopole-only—but acceptable in exchange for the dramatic reduction in complexity.

**Compatibility with Retrieval** One might hope to combine dipole corrections with retrieval for further accuracy gains. However, the natural dipole aggregation produces a single correction per query cluster by weighting each  $\text{Cov}_j(v, k)$  according to how much that query cluster attends to each key cluster. When retrieval then selects specific key clusters for exact attention computation, those clusters have already contributed to the aggregated dipole term. Correctly combining the two would require subtracting out the retrieved clusters' contribution from the dipole before adding the exact attention—possible, but complex. Given that retrieval alone already provides larger accuracy gains than dipoles, we opted not to pursue this combination.

**Empirical Comparison with Retrieval** In practice, we found that retrieval of high-attention clusters provides bet-

ter accuracy than dipole corrections. At K128, monopole-only approximation achieves 0.0227 relative squared error; adding dipole corrections reduces this to 0.0150 ( $1.5 \times$  improvement), while adding retrieval instead reduces it to 0.0062 ( $3.6 \times$  improvement). We therefore use retrieval in our main experiments.

## C. Clustering Details

We use streaming K-means to obtain cluster centroids, followed by a final assignment pass.

**Centroid Computation** Centroids are computed globally across the entire sequence. Given  $N$  input vectors (queries or keys), we compute  $K$  cluster centroids as follows:

1. **Initialization:** Shuffle inputs with a fixed random seed, then uniformly subsample every  $\lfloor N/K \rfloor$ -th vector to obtain  $K$  initial centroids.
2. **Streaming update:** Process all  $N$  vectors in a single pass using minibatches of 64 vectors. For each minibatch, compute similarities to current centroids using tensor cores, then assign each vector to its nearest centroid. For each assigned vector  $x$ , update the centroid total and count as  $t \leftarrow \beta \cdot t + x$  and  $c \leftarrow \beta \cdot c + 1$  (with  $\beta = 0.9$ ), processing assignments sequentially within the minibatch. The centroid is recovered as  $t/c$ .

A single pass suffices because the effective sample size per cluster grows with sequence length; at 64k tokens with 128 clusters, each cluster sees  $\sim 500$  vectors on average. All clustering computations use float16 precision for efficiency.

**Balanced Assignment** After computing global centroids, assignment is performed independently within each spatial block. Each vector is assigned to its nearest centroid subject to a maximum cluster size of  $4 \times B/K$  per block, where  $B$  is the spatial block size. This static cap simplifies prototyping with pure JAX implementations; the final Pallas kernels could handle variable cluster sizes but we retain the cap for consistency. The  $4 \times$  average factor was chosen empirically as it rarely binds in practice. Squared distances are computed efficiently via the identity  $\|x - c\|^2 = \|x\|^2 - 2\langle x, c \rangle + \|c\|^2$ , where  $\|x\|^2$  terms cancel when comparing distances to different centroids.

**Centroid Gradient Flow** When computing attention from query centroids (for exponential tilting), we stop gradients from flowing back through the centroid to its constituent queries. This prevents queries from being trained to “cluster well,” a property that provides no benefit when switching to exact attention at test time. We found this reduces adaptation effects.

## D. Hyperparameters

**Model Architecture** We use a standard decoder-only transformer with pre-norm (layer normalization before attention and FFN), RoPE position encodings with base frequency  $10^5$ , and embedding tying. Model sizes are parameterized by a scale factor  $S \in \{3, 4, 5, 6, 8\}$  corresponding to  $\{96\text{M}, 185\text{M}, 350\text{M}, 560\text{M}, 1\text{B}\}$  parameters:

- Embedding dimension:  $256 \times S$
- Attention heads:  $4 \times S$  (head dimension 64)
- FFN dimension:  $1024 \times S$
- Layers: 10, 12, 16, 18, 20 for scales 3–8 ( $\approx 3S$ , rounded to even for layer pairing)
- Vocabulary size: 32768
- Context length: 64k tokens

Layers are grouped into super blocks of 2: one local attention layer (sliding window of 256 tokens) followed by one global attention layer. FFN uses ReLU activation. Layer normalization uses  $\epsilon = 10^{-6}$ .

**Optimizer** We use AdamW with  $\beta_1 = 0.9$ ,  $\beta_2 = 0.95$ ,  $\epsilon = 10^{-6}$ , and weight decay 0.01. Gradients are clipped to global norm 1.0. Learning rate follows a warmup-cosine schedule with 4000 warmup steps and final value 10% of peak. Peak learning rate is  $3 \times 10^{-3}$ , scaled by  $S^{-0.5}$ .

**Training Data** We train on two datasets:

- **Code:** The Stack v2 (Lozhkov et al., 2024) ([bigcode/the-stack-v2-train-smol-ids](#)). We filter to Python files, excluding vendor and generated code. Repositories are bucketed by estimated token count (Python bytes / 3.5) on a  $\log_2$  scale; we use buckets 5–8 corresponding to 16k–256k tokens per repository. Files within each repository are concatenated with `<reponame>` and `<filename>` delimiters, sorted by path depth. Total: 21.5B tokens.
- **Scientific documents:** OLMo 3 LongMino pool (Olmo et al., 2025) ([allenai/dolma3\\_longmino\\_pool](#)), science\_tech topic, bucket 2e16 (64k–128k tokens per document). Total: 37.5B tokens.

Both datasets use separate BPE tokenizers with 32768 vocabulary trained on domain-specific samples. Training token counts scale with model size: 2.0B, 4.0B, 7.5B, 12.9B, and 23.6B tokens for scales 3–8 respectively. Batch size is 2 sequences of 64k tokens (128k tokens per step).

**MuSe Operating Point** For pretraining experiments, we use 128 query clusters, 128 key clusters, top-8 cluster retrieval, top-1 spatial block retrieval, and 8k spatial blocks (Q128K128R8SP1B8k). This configuration achieves <1% relative squared error on microbenchmarks while providing 2 $\times$  speedup over CUDNN Flash Attention.

**Hardware** All pretraining experiments use 8 $\times$  NVIDIA A100 (80GB) GPUs in a (2, 4) mesh with data parallelism over the batch dimension and model parallelism over attention heads. Training uses mixed precision (bfloating16/float32).

**Llama Evaluation** For generalization experiments (Section 4.3), we evaluate on pretrained Llama 3.2 1B and Llama 3.1 8B models converted to Flax. We measure per-position cross-entropy loss on PG-19 (Rae et al., 2020) (test split) with 64k context, using 100 document chunks. Cumulative mean loss is computed across positions and plotted as reducible loss (subtracting fitted irreducible loss).

**Approximation Quality Metric** We report relative squared error (RSE) as our primary measure of approximation quality:  $RSE = \|o_{\text{approx}} - o_{\text{exact}}\|^2 / \|o_{\text{exact}}\|^2$ , where  $o$  denotes the attention output, averaged across all queries in the evaluation batch.

## E. 96M Model Microbenchmarks

This appendix presents detailed microbenchmark results from a 96M parameter model. We evaluate approximation quality on queries, keys, and values extracted from the trained model with 64k context. We use 2 sequences across all 60 attention heads (from all layers), with head dimension 64. Our base configuration uses 128 query clusters, 128 key clusters, top-8 cluster retrieval, top-1 spatial block retrieval, and 8k spatial blocks (Q128K128R8SP1B8k).

### E.1. Speedup vs Exact Attention

Table 8 compares MuSe to exact flash attention implementations. At our base configuration (QK128R8), MuSe achieves 2 $\times$  speedup over CUDNN Flash Attention with 2.6% relative squared error.

Table 8. Runtime comparison with exact attention (64k context, head dim 64, 96M model).

Method	Time (ms)	Speedup	RSE
CUDNN Flash	212.1	1.0 $\times$	0 (exact)
Pallas Flash	243.6	0.87 $\times$	0 (exact)
MuSe QK64R8	118.1	1.80 $\times$	0.0315
MuSe QK128R8	105.5	2.01 $\times$	0.0259
MuSe QK256R8	123.3	1.72 $\times$	0.0206

### E.2. Effect of Query Clustering

Table 9 shows the effect of varying the number of query clusters while holding other parameters fixed. Reducing from 128 to 1 query cluster (mathematically equivalent to no query clustering) increases relative squared error by 1.9 $\times$  (0.026 to 0.049) with negligible runtime difference, validating the importance of query clustering.

Table 9. Effect of query cluster count (K128R8SP1B8k fixed). Q1 uses zeroed centroids, mathematically equivalent to no query clustering.

Q	RSE	Correlation	Time (ms)
256	0.0214	0.9875	122.6
128	0.0259	0.9848	105.5
64	0.0301	0.9825	104.3
32	0.0338	0.9764	102.0
16	0.0376	0.9737	103.6
1*	0.0494	0.9685	105.6

### E.3. Effect of Key Clustering

Table 10 shows the effect of varying key clusters with retrieval fraction held constant (R/K = 1/16). More clusters with proportionally more retrieval improves accuracy, with K128R8 providing a good speed/accuracy tradeoff.

Table 10. Effect of key cluster count with fixed retrieval fraction (Q128SP1B8k fixed, R/K = 1/16).

K	R	RSE	Correlation	Time (ms)
256	16	0.0180	0.9882	137.1
128	8	0.0259	0.9848	105.5
64	4	0.0359	0.9762	106.7
32	2	0.0504	0.9639	117.8
16	1	0.0692	0.9539	126.1

### E.4. Joint Query and Key Clustering

Table 11 compares performance with and without query clustering as the number of key clusters varies. Query clustering provides 1.4–2.4 $\times$  error reduction, with larger benefits at higher cluster counts where query-specific summaries matter more.

Table 11. Effect of query clustering across key cluster counts (R/K = 1/16, SP1B8k fixed). “No Q” uses zeroed query centroids.

K	R	RSE		Corr		Gain
		No Q	With Q	No Q	With Q	
256	16	0.0365	0.0152	0.9749	0.9891	2.4 $\times$
128	8	0.0494	0.0259	0.9685	0.9848	1.9 $\times$
64	4	0.0676	0.0414	0.9541	0.9723	1.6 $\times$
32	2	0.0943	0.0640	0.9400	0.9576	1.5 $\times$
16	1	0.1295	0.0933	0.9177	0.9373	1.4 $\times$

### E.5. Monopole Only (No Retrieval)

Table 12 shows performance without retrieval, comparing monopole approximation with and without query clustering. Query clustering provides  $1.9\text{--}2.7\times$  error reduction for monopole-only—larger than the  $1.4\text{--}2.4\times$  benefit observed with retrieval (Table 11). This confirms that query clustering is most critical for the monopole component; retrieval partially masks the benefit by handling high-attention clusters exactly.

Table 12. Monopole only (no retrieval), with and without query clustering. “No Q” uses zeroed query centroids.

QK	RSE		Corr		Gain
	No Q	With Q	No Q	With Q	
256	0.1560	0.0586	0.9005	0.9606	$2.7\times$
128	0.1812	0.0794	0.8879	0.9430	$2.3\times$
64	0.2118	0.1025	0.8697	0.9283	$2.1\times$
32	0.2362	0.1273	0.8578	0.9131	$1.9\times$

### E.6. Cluster Count vs Retrieval Work

Table 13 shows a striking result: increasing cluster count improves accuracy while *reducing* retrieval work. With  $R=8$  fixed, each doubling of cluster count improves error by  $1.2\text{--}1.3\times$  while halving the number of keys retrieved per query. QK512R8 achieves  $2\times$  better accuracy than QK64R8 while retrieving  $8\times$  fewer keys. This demonstrates that finer clustering improves monopole quality enough to more than compensate for retrieving from smaller clusters.

Table 14 shows the effect of varying retrieval count with cluster count fixed. Doubling retrieval from  $R=8$  to  $R=16$  improves error by  $1.27\times$ —comparable to the  $1.26\times$  improvement from doubling cluster count (QK128 to QK256) at fixed  $R=8$ .

Table 13. Effect of cluster count with fixed retrieval count  $R=8$  (SP1B8k fixed). Higher cluster counts improve accuracy despite less retrieval work.

QK	R	RSE	Correlation	Keys/query	Time (ms)
512	8	0.0156	0.9908	1024	226.0
256	8	0.0206	0.9887	2048	123.3
128	8	0.0259	0.9848	4096	105.5
64	8	0.0315	0.9789	8192	118.1

Table 14. Effect of retrieval count with fixed cluster count (QK128SP1B8k fixed).

QK	R	RSE	Correlation	Time (ms)
128	16	0.0204	0.9851	140.8
128	8	0.0259	0.9848	105.6
128	4	0.0355	0.9739	89.6

### E.7. Retrieval Only (No Monopole)

Table 15 shows performance with retrieval only, disabling the monopole contribution. Query clustering provides only  $1.07\times$  benefit for retrieval selection, compared to  $2.3\times$  for monopole-only (Table 12). This confirms that query clustering primarily improves monopole quality; the retrieval mechanism selects reasonable clusters even without query-specific summaries. Importantly, query clustering does not harm retrieval, making it a pure win.

Table 15. Retrieval only (no monopole) at QK128R8SP1B8k. “No Q” uses zeroed query centroids.

Setting	RSE	Correlation	Time (ms)
With Q	0.0990	0.9645	103.4
No Q	0.1061	0.9556	103.2
Q benefit		$1.07\times$	

## F. 1B Model Microbenchmarks

This appendix presents detailed microbenchmark results from our 1B parameter model (320 heads, head dimension 64, 64k context). These experiments validate hyperparameter choices and characterize approximation quality at scale.

### F.1. Block Size and Spatial Retrieval Tradeoff

Table 16 shows the effect of varying block size  $B$  while adjusting spatial retrieval  $SP$  to maintain constant retrieval span ( $SP \times B = 16k$ ). With cluster count and cluster retrieval fixed (QK128R4), this sweep illustrates the fundamental tradeoff between exact local attention and approximate far-field attention.

Table 16. Effect of block size with constant retrieval span (QK128R4,  $SP \times B = 16k$ , 1B model, 40 heads, 2 sequences). Larger blocks compute more attention exactly but have higher diagonal cost; smaller blocks approximate more attention but eventually become slow due to accumulation overhead.

Config	RSE	Correlation	Time (ms)
QK128R4SP1B16k	0.00493	0.9974	105.6
QK128R4SP2B8k	0.00704	0.9959	75.5
QK128R4SP4B4k	0.01578	0.9901	71.8
QK128R4SP8B2k	0.03833	0.9767	129.4

Accuracy degrades as block size decreases ( $0.00493 \rightarrow 0.03833$ , a  $7.8\times$  increase in error) because more of the attention mass—which is predominantly local—must be routed through the approximation rather than computed exactly in the block diagonal.

Runtime exhibits a U-shape:  $B = 4k\text{--}8k$  is fastest ( $\sim 72\text{--}76$ ms), while both  $B = 16k$  (expensive diagonal attention) and  $B = 2k$  (expensive accumulation over 32 blocks plus 8

spatial selections per query) are slower. This demonstrates that block size provides a tunable speed/accuracy tradeoff, with  $B = 8k$  offering a good balance for 64k context.

We use  $SP = 1$  (single spatial block per cluster) for simplicity;  $SP = 2$  with reduced cluster retrieval ( $R = 4$ ) shows similar microbenchmark performance but exhibited more adaptation during pretraining.

## F.2. Cluster Count with Fixed Retrieval

Table 17 shows the effect of varying cluster count with retrieval count held fixed at  $R=8$ . Higher cluster counts improve accuracy ( $0.00838 \rightarrow 0.00456$ , a  $1.8\times$  error reduction) while reducing retrieval work ( $8192 \rightarrow 2048$  keys per query). This confirms the 96M result (Table 13): finer clustering improves monopole quality enough to more than compensate for retrieving from smaller clusters.

Table 17. Effect of cluster count with fixed retrieval  $R=8$  (SP1B8k, 1B model, 80 heads, 2 sequences, 64k context).

Config	RSE	Correlation	Keys/query
QK64R8	0.00838	0.9949	8192
QK128R8	0.00622	0.9965	4096
QK256R8	0.00456	0.9975	2048

## F.3. Monopole Runtime Scaling

We measure monopole-only runtime (no retrieval) to characterize the scaling of the novel MuSe components: clustering, summary computation, and causal accumulation. All timings are for 40 heads on a single node (5 heads per A100).

**Sequence Length at Constant Total Tokens** Table 18 shows monopole runtime at constant total tokens (128k) but varying sequence length and batch size. Longer sequences are modestly slower despite equal total work, likely due to reduced parallelism across sequences or less efficient clustering on larger point sets rather than algorithmic overhead.

Table 18. Monopole-only runtime at constant total tokens (128k), varying sequence length (QK128B8k, 40 heads).

Config	Sequences	Blocks/seq	Time (ms)
N=32k	4	4	33.3
N=64k	2	8	36.0
N=128k	1	16	41.0

Per-token cost increases modestly with sequence length:  $0.26 \mu\text{s}/\text{token}$  at 32k context to  $0.32 \mu\text{s}/\text{token}$  at 128k context ( $+23\%$ ). This is slightly super-linear in sequence length at constant batch size, but the overhead is mild.

**Cluster Count Scaling** Table 19 shows monopole runtime as cluster count varies at fixed context length. Increasing

clusters from 64 to 256 ( $4\times$ ) increases runtime by only 31%, indicating that cluster-dependent costs (summaries, accumulation) are not dominant.

Table 19. Monopole-only runtime varying cluster count (B=16k, N=64k, 40 heads, constant total tokens via batching).

Clusters	Time (ms)	vs QK64
QK64	52.1	—
QK128	55.3	+6%
QK256	68.3	+31%

If accumulation (which scales as  $C^2$ ) dominated, we would expect  $4\times$  clusters to yield  $16\times$  runtime; the observed 31% increase confirms that accumulation is a small fraction of total monopole cost.

**Sequence Length with Larger Blocks** Table 20 shows a similar experiment with B=16k blocks and QK64.

Table 20. Monopole-only runtime at constant total tokens (128k), varying sequence length (QK64B16k, 40 heads).

Config	Sequences	Blocks/seq	Time (ms)
N=32k	4	2	49.4
N=64k	2	4	52.1
N=128k	1	8	57.9

The pattern is consistent: longer sequences are slower at constant total tokens (+17% from 32k to 128k), but the overhead is modest and likely attributable to reduced parallelism or clustering efficiency rather than algorithmic complexity.

## F.4. Comparison with MoBA

The main text compares MuSe against MoBA at matched far-field sparsity (8k block diagonal,  $64\times$  sparsity), isolating the quality of far-field approximation. For completeness, we also compare against MoBA with settings closer to typical usage: 512-token block diagonal with top-8 retrieval from 512-token blocks ( $8\times$  far-field sparsity). This configuration allocates more compute budget to far-field retrieval at the cost of local attention quality.

Table 21 shows that even under these favorable conditions, MuSe maintains an advantage at both scales. Note that this comparison favors MoBA: our 8k block size is chosen to balance accuracy and runtime with our kernels, not to maximize sparsity. The 512-block MoBA configuration would be substantially slower than exact attention when implemented with our kernels.

## F.5. Far-Field Scaling with Context Length

Table 22 shows approximation quality versus context length with scaled hyperparameters:  $QK \propto \sqrt{N}$ ,  $R \propto \sqrt{N}$  (constant retrieval fraction),  $B \propto N$  (constant 8 spatial blocks).

Table 21. Extended MoBA comparison at 185M and 560M scale. “Sparsity-matched” uses 8k block diagonal with  $64 \times$  far-field sparsity; “Budget-matched” uses 512-token blocks with  $8 \times$  far-field sparsity. Cross-entropy loss, lower is better.

Scale	Method	Test Attention	
		CUDNN	Method
185M	CUDNN (baseline)	0.9400	—
	MuSe	<b>0.9384</b>	0.9435
	MoBA (sparsity-matched)	0.9714	1.0027
	MoBA (budget-matched)	0.9460	0.9633
560M	CUDNN (baseline)	0.7745	—
	MuSe	<b>0.7728</b>	0.7746
	MoBA (sparsity-matched)	0.7958	0.8209
	MoBA (budget-matched)	0.7815	0.7858

This maintains  $64 \times$  far-field sparsity and 1/8 block diagonal fraction across all context lengths.

Table 22. Far-field approximation quality vs. context length with scaled hyperparameters (8 spatial blocks throughout). Relative squared error decreases as context grows. \*128k context created by concatenating two 64k sequences.

<i>N</i>	QK	<i>R</i>	<i>B</i>	RSE	Cosine
<i>Series 1:</i>					
4k	32	2	512	0.00884	0.9947
16k	64	4	2k	0.00662	0.9958
64k	128	8	8k	0.00622	0.9965
<i>Series 2:</i>					
2k	16	1	256	0.01701	0.9899
8k	32	2	1k	0.01096	0.9929
32k	64	4	4k	0.00863	0.9946
128k*	128	8	16k	0.00723	0.9956

Approximation error decreases substantially with scale ( $0.017 \rightarrow 0.007$  from 2k to 128k), implying that the compute required to achieve a given error level grows sub-quadratically in the far-field. We do not determine the precise exponent, which would likely be data-dependent. The block diagonal cost remains  $O(N^2/S)$ ; for very long contexts where this dominates, recursive application of MuSe would reduce it further.

## G. Additional Results

### G.1. Effective Cluster Count Comparison

Tables 23 and 24 compare MuSe and the no-query-clustering ablation by computing effective cluster counts. For each configuration, we interpolate (or extrapolate) using a power-law fit to determine what cluster count the other method would require to achieve the same error. Both methods follow approximate power laws: MuSe with exponent  $d \approx -0.89$  and no-query-clustering with  $d \approx -0.59$ . The steeper slope for MuSe means its advantage grows with cluster count.

Table 23. MuSe configurations with equivalent no-query-clustering cluster counts.  $R = QK/16$  throughout. Effective cluster count interpolated via power-law fit. Multiplier shows how many more clusters the no-query-clustering method would need.

QK	RSE	Corr	Eff. No-Q	Mult.
16	0.0380	0.9775	82	5.1 $\times$
32	0.0210	0.9878	191	6.0 $\times$
64	0.0114	0.9935	568	8.9 $\times$
128	0.0062	0.9965	1179	9.2 $\times$
256	0.0033	0.9980	2518	9.8 $\times$
512	0.0017	0.9990	5481	10.7 $\times$

Table 24. No-query-clustering configurations with equivalent MuSe cluster counts.  $R = QK/16$  throughout. Multiplier shows how many fewer clusters MuSe needs to achieve the same error.

QK	RSE	Corr	Eff. MuSe	Mult.
16	0.0991	0.9464	6	2.7 $\times$
32	0.0665	0.9640	9	3.6 $\times$
64	0.0428	0.9775	13	4.9 $\times$
128	0.0284	0.9856	19	6.7 $\times$
256	0.0191	0.9904	36	7.1 $\times$
512	0.0129	0.9935	57	9.0 $\times$

### G.2. Downstream Evaluation

To verify that MuSe does not degrade downstream task performance, we evaluate 1B models trained on scientific PDFs using the lm-eval harness on ARC-Easy and SciQ. Table 25 shows that MuSe-trained models perform comparably to CUDNN-trained models, with all differences within one standard error. Both models are well above the 25% random baseline, confirming that the approximation does not impair learned representations.

Table 25. Downstream evaluation on ARC-Easy and SciQ (1B model trained on scientific PDFs). All differences are within standard error ( $\sim 0.01$ ).

Benchmark	Metric	CUDNN	MuSe
ARC-Easy	acc	0.479	0.487
ARC-Easy	acc_norm	0.431	0.436
SciQ	acc	0.766	0.759
SciQ	acc_norm	0.663	0.659

### G.3. Fine-tuning to Remove Adaptation

At 1B scale on the code domain, the MuSe-trained model shows minor adaptation to the approximation: when evaluated with CUDNN attention, loss is 0.7108 compared to the baseline of 0.7026. We investigate whether brief fine-tuning with exact attention removes this adaptation.

Table 26 shows the progression of MuSe  $\rightarrow$  CUDNN evaluation loss during CUDNN fine-tuning. The adaptation gap closes rapidly: after just 26M tokens (0.1% of pretraining), the model not only matches but *beats* the CUDNN

baseline (0.6994 vs 0.7026). Continued fine-tuning yields diminishing returns, with 93% of the improvement occurring in the first 0.1% of fine-tuning tokens. This confirms that adaptation effects are shallow and easily removed, making the recommended workflow straightforward: pretrain with MuSe for speedup, then briefly fine-tune with exact attention before deployment.

Table 26. Fine-tuning progression on 1B code model. MuSe → CUDNN evaluation loss during CUDNN fine-tuning.

MTok	% Pretrain	Loss	Note
0	0%	0.7108	Before fine-tuning
26	0.1%	0.6994	Beats baseline (0.7026)
210	0.9%	0.6985	Continued improvement

#### G.4. Distributed Training Considerations

MuSe is compatible with standard distributed training strategies.

**Sequence parallelism** In Megatron-style sequence parallelism, attention heads are sharded across devices, with the full sequence gathered for each head before attention. From the perspective of MuSe, each device simply approximates fewer heads over the complete sequence—the distributed origin of sequence fragments is invisible to the approximation. Our pretraining experiments use this approach.

**Ring attention** Ring attention distributes the sequence across devices, rotating key/value blocks around a ring. The block-diagonal (local, causal) attention is naturally handled by MuSe’s spatial blocking. For off-diagonal (remote, non-causal) blocks, MuSe extends naturally: either retain spatial blocking with the causal mask removed, or treat remote context as a single spatial block with purely semantic sparsity. We leave detailed investigation of these extensions to future work.